3D INDOOR CORRIDOR MAPPING WITH CALIBRATED ROPs OF A MULTI-FISHEYE CAMERA-RIG

Muhammad Syafiq[1], Jiann-Yeou Rau[1], Jyun-Ping Jhan[2]

1 Department of Geomatics, National Cheng Kung University, Taiwan – P66097076@gs.ncku.edu.tw and jyrau@geomatics.ncku.edu.tw
2 Taiwan Building Technology Center, National Taiwan University of Science and Technology, Taiwan – jpjhan@mail.ntust.edu.tw

Commission II

KEY WORDS: Camera Calibration, Multi-Fisheye Camera-rig, Relative Orientation Parameters, 3D reconstruction.

ABSTRACT:

We present a 3D indoor mapping simulation in the location with limitations to access (i.e., pipeline drainage, sewer, box girder, etc.) by utilising a multi-fisheye camera rig. This camera rig (i.e., Pilot One) offers a 360 Field of View (FoV) coverage that represents an efficient data acquisition solution. Particular attention is focused on camera calibration consists of Interior Orientation Parameters (IOPs) and Relative Orientation Parameters (ROPs) to generate an accurate 3D reconstruction result. An appropriate Self-Calibration Bundle Adjustment (SCBA) approach, assisted with Australis coded targets, is conducted to have stable pre-calibration parameters that can be applied in a 68 meters corridor study field. We performed forward and backward data acquisition with unstitched original images and stitched images separately in a straight line to simulate data acquisition for future applications. However, due to the camera model and uncalibrated images, there is a “banana effect” in the stitched image. Twenty scale bars are used in this study. To achieve the ideal position and orientation of the scale bars, we attempt to construct a number of scenarios. The objective of this simulation is to determine the minimum number of scale bars that can be applied to a corridor where is difficult to access. We try to set up without any Control Scale Bars (CSB) with 20 Check Scale Bars (CkSBs). Even though this trial only has a 3.8 cm CkSBs error, it produced a length estimation error of 2.3 m (i.e., 3.37% of 68.1m) when compared with Terrestrial Laser Scanning.

1. INTRODUCTION

1.1 Rise of 360 action multi-camera systems

In recent years, 3D indoor mapping has grown increasingly along with the high demand for digital archiving, infrastructure monitoring, metaverse applications, indoor navigation, etc. Furthermore, sensor technology has rapidly changed due to consumer-grade and easy-to-operate requirements from the market (Hasler et al. 2019). Indoor 3D model generation is commonly reconstructed by a single-camera or terrestrial laser scanning (TLS). However, utilizing a single camera that does not provide a sufficient angular field of view (FOV) requires more scene captures to cover the whole indoor environment. Meanwhile, data acquisition using TLS has a minimum distance to scan the environment, so it has limitations on data acquisition in a narrow space and sometimes cannot offer images for visual inspection. In addition, TLS also has limitations due to high costs during data acquisition (Fiorillo, et al., 2016).
As a practical response, a low-cost instrument represented by a consumer-grade camera-rig is suggested for generating indoor 3D models. A four-fisheye camera-rig with a total of 360-degree FOV, i.e., Pilot One, provides an effective and efficient solution for indoor image acquisition, especially in the location that are difficult-to-access (Lari et al. 2014), such as underground sewers, the interior of a box girder bridge, etc. However, this multi-fisheye camera-rig is inseparable from large lens distortions at the edges of the original image. To deal with this issue, it is necessary to pre-calibrate all four cameras in order to obtain appropriate and stable camera parameters for accurate 3D model generation. Furthermore, the Relative Orientation Parameters (ROPs) that contain base-lines between cameras can offer a scale factor of the generated 3D model, which is important for an area where establishing ground controls is not easy. The suggested calibration method estimates the Interior Orientation Parameters (IOPs) for each camera to define the internal geometry of the camera as well as the ROPs to define the relative spatial offsets and rotation angles between the master camera and three slave ones (Detchev et al. 2014).

1.2 Pilot One Multi Fisheye Camera-Rig

Nowadays, two types of consumer-friendly 360-degree cameras are available on the market. One is equipped with a single lens in a panoramic camera, whereas the other one is a multi-lens configuration (Abate et al. 2017). A pocket-size and lightness multi-fisheye camera rig (i.e., Pilot One) with 44 x 44 x 127 mm size and a weight of 395 gr also allows for portable data acquisition. The camera is equipped with a 12 MP optical sensor and provides (3648 × 2280) pixels in 8K unstitched video while it has (3840 × 1920) pixels in 8K stitched video, which is able to offer sufficient image resolution for 3D reconstruction purposes. Furthermore, it features aperture (f/2.28) and a 1.88 mm focal length, providing 185-degrees Field of View (FoV) per lens. Therefore, the Pilot One multi-fisheye camera rig is suitable to use in the study area with limitations to access. In addition, this camera offers rolling shutter compensation that can support dynamic or moving during data acquisition.

1.3 Paper objectives and challenges

This research proposed a pre-calibration procedure for a multi-fish eye camera rig and applied it along a corridor area. Due to efficiency and fast data acquisition purposes, we utilize unstitched video and stitched video sequenced features from Pilot One separately. Then, unstitched videos were extracted to unstitched images for pre-calibration purposes whereas the stitched videos were extracted to stitched panoramic images in a spherical mode for comparison. A pre-calibration procedure was performed by utilising Self Calibration Bundle Adjustment

https://doi.org/10.5194/isprs-archives-XLVIII-2-W1-2022-237-2022

(SCBA) methods and applied to the unstitched original images. The selected area is in an indoor corridor area with dimensions (68.1 x 1.8 x 2.4) meters with a homogeneous object, especially on the ceiling and on the wall. This environment was selected to simulate data acquisition for future applications in an extreme area study (i.e., box girder). For accuracy assessment, this study also acquires TLS scanning for reference. Sony α7R2 acquisition in the area of study and other corridor areas with more features was carried out to further demonstrate the impact of calibrated ROPs in the multicamera rig in the homogeneous object. In the end, we performed several Control Scale Bars (CSBs) and Check Scale Bars (CkSBs) scenarios with different amounts and various positions and orientations because attempting the scale bars requires more time and effort, especially in locations where access is difficult.

2. METHODOLOGY

2.1 Camera calibration parameters

This study utilizes the Pilot One multi-fisheye camera-rig, which comprises four lenses in a hard and firm box. For precise image measurement, camera calibration is a crucial step in lens distortion correction. To perform SCBA with additional parameters, Australis coded markers are also utilized (Clive S.Fraser 1997).

2.1.1 Interior Orientation Parameters (IOPs)

Non-metric digital cameras have unstable interior orientation parameters and high lens distortion values, in contrast to metric cameras, which are made specifically for photogrammetric applications and have very stable interior orientation parameters and low lens distortion values (Fraser, 2006). Interior orientation describes a camera's internal geometries as they were at the time of image capture. These parameters include the camera's calibrated principal distance or the lens's focal length, the principal point's location in the image plane (x, y), and lens distortion parameters (Pérez et al. 2012). The following internal orientation components can be extracted from non-metric cameras: calibrated focal length (f), the coordinates of the image's center of projection (xp, yp), the radial lens distortion coefficients (k1, k2, and k3), and tangential distortion coefficients (p1, p2) (Balletti et al. 2014). Camera calibration must be carried out in order to obtain trustworthy IOPs components that allows accurate 3D reconstruction (Habib et al. 2006). Equations (1) and (2) show the self-calibration bundle adjustment equations, while Equations (3) and (4) show the camera's additional parameters.

$$x - xp = -f\frac{m_{11}(X-X_0)+m_{12}(Y-Y_0)+m_{13}(Z-Z_0)}{m_{31}(X-X_0)+m_{32}(Y-Y_0)+m_{33}(Z-Z_0)} + \Delta x\,, \tag{1}$$

$$y - yp = -f\frac{m_{11}(X-X_0)+m_{12}(Y-Y_0)+m_{13}(Z-Z_0)}{m_{31}(X-X_0)+m_{32}(Y-Y_0)+m_{33}(Z-Z_0)} + \Delta y, \tag{2}$$

$$\Delta x = (x-xp)\,(K_1r^2+K_2r^4+K_3r^6)+P_1(r^2+(x-xp)^2)+2P_2(x-xp)(y-yp), \tag{3}$$

$$\Delta y = (y-yp)\,(K_1r^2+K_2r^4+K_3r^6)+P_2(r^2+(y-yp)^2)+2P_1(x-xp)(y-yp), \tag{4}$$

The following SCBA equation, (X_o, Y_o, Z_o) denotes the camera position, m_{11} are the nine elements of the camera rotation matrix, (X, Y, Z) the coordinates of image measurement (x, y) in object space, and (Δx, Δy) the amount of lens distortion correction. The focal length f, principal points (x, y), radial lens distortion parameters (K_1, K_2, K_3), and decentering parameters (P_1, P_2), where r is the distance to the center of image measurement, are all included in the IOPs (x, y) (Jyun Ping Jhan, Rau, and Chou 2020).

2.1.2 Relative Orientation Parameters (ROPs)

Each camera in the Pilot One multicamera rig system has a baseline with the others that acts as scale factor for the creation of 3D models, resulting in relative rotation angles and relative spatial offsets (as shown in Fig.1a). The fisheye camera's individual lenses slightly overlap one another it is beneficial for the alignment process (Esquivel, et al. 2007) (depicted in Fig.1b). Bright red represents horizontal FOV from the top perspective in Fig.1b, while dark red represents slight overlap for individual lenses in a multicamera-rig system.

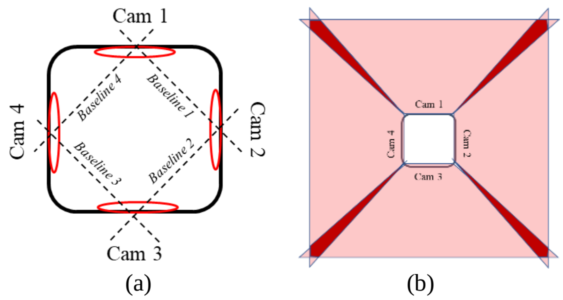

Figure 1. Multi camera rig concept: (a) corresponding between each camera (b) horizontal FoV (bright red) and overlapping between each camera (dark red).

Identifying the 3D relative rotation angles ($\Delta\boldsymbol{\omega}$, $\Delta\boldsymbol{\varphi}$, $\Delta\boldsymbol{\kappa}$) and relative spatial offset vectors ($\boldsymbol{VVxx}$, $\boldsymbol{VVyy}$, $\boldsymbol{VVzz}$) between one camera and the slave cameras in the set is the goal of the relative orientation of the cameras common problem (Wierzbicki 2018). In our proposed sensor, Camera 1 serves as the reference camera, whereas the other cameras are determined as slaves. Equations (5) represent the rotation matrix between two cameras, whereas Equations (6) describe the position vector between two cameras in perspective centers.

$$R_{CM}^{CS} = R_M^{CS} \text{x}\, R_{CM}^M\,, \tag{5}$$

$$r_{CM}^{CS} = R_{CS}^M \ \text{x}\ (r_{CS}^M - r_{CM}^M)\,, \tag{6}$$

From the equation above, relative orientation angles were calculated by R_{CM}^{CS}. It denotes the rotation matrix between the two cameras is a coordinated system in the local mapping frame M, where C_M is represented as the master camera and C_S is represented as the slave camera, respectively. The position vector between the perspective centers of two cameras, represented by r_{CM}^{CS} calculations, was used to derive the offset vector (Vx, Vy, and Vz). The mean of ROPs from multiple stations and their standard deviation are used for pre-calibration initial values and internal accuracies of calibration results (J. P.Jhan et al 2015).

2.2 Camera Pre-calibration

Pre-calibration methods were adopted, due to the overlap and convergent angle limitations that prevented a lack of geometrical network during acquisition and for subsequent applications (Jiang et al. 2017). We calibrate the cameras using extracted images from the Pilot One video with 8K resolutions. First, to acquire a precise and accurate 3D calibration field that is fully covered by lots of Australis coded targets. We captured numerous images with the Sony RX-10 (9mm focal length) and estimated all images' Exterior Orientation Parameters (EOPs) and all coded targets' 3D coordinates by SCBA (Dawson et al. 2017; Fraser & Edmundson, 2000). In order to increase the accuracy and stability of camera calibration by obtaining different convergent angles, the Pilot One camera-rig image acquisition was also carried out in the same room by capturing images in many directions, i.e., rotating 45 degrees at each station along with landscape and portrait orientations (as shown in Fig. 2) (Perez et al. 2022).

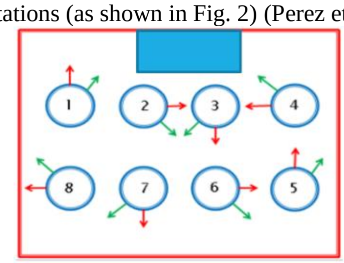

Figure 2. Data acquisition illustration for multi-camera calibration purposes in a calibration room.

A total of 96 original images from the Pilot One multicamera rig were used to create 24 pairs images. For comparison, we also conducted the Structure from Motion (SfM) algorithm together with SCBA to derive EOPs/IOPs and ROPs (AlKhalil 2020), in which the ground control points (GCPs) are provided by Sony RX-10 images' SCBA results. In total, 427 Australis coded targets' GCPs were used to obtain accurate scale factor and the calibrated parameters (Fig. 2). Once it was established that IOPs for each camera and the ROPs between the reference camera and the three slaves were stables and appropriate, then were used as the calibration initial value for numerous subsequent application and additional difficult area studies.

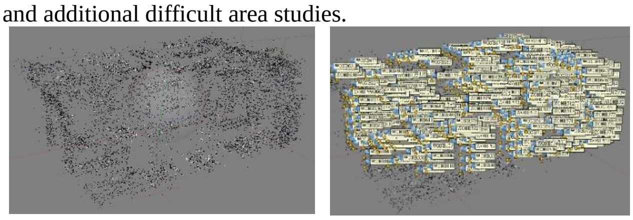

a. Sparse point cloud after aerial triangulation. b.Distribution of GCPs obtained by Australis coded targets.

Figure 3. SfM and SCBA results.

2.3 Data Acquisition in a long corridor

The image acquisition plan will be conducted in a straight line in future applications, including box-girder interior inspection. Thus, in this study, we simulate image acquisition along a long corridor with forward and backward directions. This approach was chosen because it doesn't require collecting data surrounding the corridor in the same way that a single camera acquisition does. In this case, acquisition stability and speed were prioritized during data acquisition to prevent blurry original images. For comparison, we acquire images with unstitched original images and stitched spherical panoramic images. We utilize pre-calibrated IOPs and ROPs during the EOPs estimation for the unstitched original images. A total of 20 scale bars (10 horizontal orientation & 10 vertical orientation) were well distributed along a 68 meters corridor (Yamafune, 2017) (as shown in Fig.4). In Fig.4 the numbers 1 through 20 represent vertical orientations, while the numbers 21 through 40 are noted in horizontal orientations.

We try to configure several scenarios to perform the best position and orientation of scale bars. In that sequence, we use 8 CSBs and 12 CkSBs in both horizontal and vertical orientations. Five CSBs and 15 CkSBs were applied horizontally. After that, we generated two CSBs and 18 CkSBs were used with all horizontal, all vertical, and one vertical and one horizontal. The objective of this simulation is to determine the minimum number of scale bars that can be applied to a corridor that is difficult to access. Meanwhile, in the stitched images, some commercial photogrammetry software (i.e., Metashape) is able to support spherical camera model along with various lens developments in addition (Barazzetti et al. 2017). Both these two cases are used to build dense point cloud and 3D model reconstruction. For accuracy assessment, we utilize TLS to obtain 3D point cloud data as a reference. Although we are using seven stations for this acquisition, the point cloud with a one-meter radius from the stations cannot be obtained due to TLS's minimum distance requirements. Additionally, data collection with the Sony α7R2 (24mm focal length) was carried out by capturing every part of the corridor area (such as ceiling, floors, and the wall) with more images. However, even though this camera has a greater resolution, it took more time and more effort during data acquisition along the corridor with limitations in space.

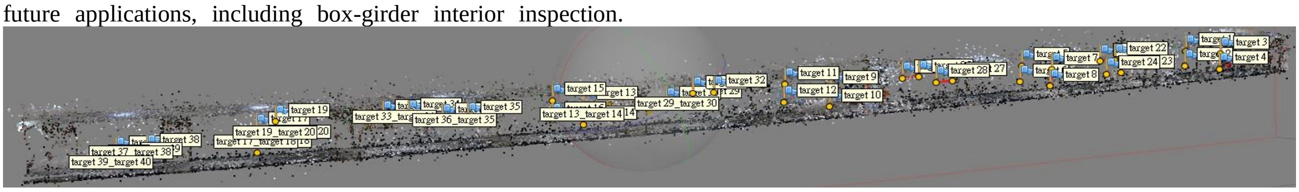

Figure 4. Scale bars distributions (target 1-20 vertical orientations & 21-40 horizontal orientations).

2.4 Data processing

High spatial resolution dense point clouds can be automatically generated by a multicamera rig system and the SfM-MVS pipeline. In this study, Agisoft Metashape was adopted to implement these algorithms. Moreover, Metashape is also able to support some specific camera models, such as fisheye lenses, multicamera rig systems, and spherical camera models to fit various characteristics of lens distortions. We use a spherical camera model without any calibration in the stitched images. Whereas employing a fisheye camera model and inputting an IOPs pre-calibration value for each camera in the unstitched images. The ROPs pre-calibration is then set as an initial value, and a standard deviation value as well. Then, SCBA methods are used to generate sparse clouds and resolve the intrinsic and extrinsic orientation of the camera. Following the automatic detection of the Metashape markers, measured scale bars were added with an input orientation of 1.1 meter horizontally and one meters vertically. Furthermore, to determine the minimum CSBs that can be applied for future applications and to perform how appropriate pre-calibration parameter values, several scalebar scenario configurations were conducted. Finally, SfM step was followed by the application of the MVS algorithm to produce dense point clouds. For additional analysis, we also processed acquired data in the same study area, which has homogeneous objects, and also in a corridor with more features from Sony α7R2 camera, respectively.

3. RESULTS AND DISCUSSION

3.1 Camera calibration

Based on camera calibration through bundle adjustment, we were able to determine the IOPs value for each fisheye lens and the

ROPs values for relative spatial offsets, which include x, y, and z coordinates and standard deviation between the master camera and three slave ones, respectively (as shown in Table 1). Furthermore, Pilot One's master camera and three slave cameras were measured for their relative rotation angles, which are: Omega (ω) the rotation around the X axis, Phi (φ), the rotation around the Y axis, and Kappa (κ), the rotation around the Z axis (as shown in Table 2). Next, we utilize the IOPs/ROPs parameter's initial value to generate 3D models from multicamera-rig.

Table 1. Relative spatial offsets.

Master Cam1	Spatial Offsets (mm)			Std. Dev. (mm)		
	X	Y	Z	X	Y	Z
Slave Cam 2	-0.99	-13.25	-44.09	8.70	8.60	10.81
Slave Cam 3	-0.13	-27.48	-15.29	8.46	9.42	9.61
Slave Cam 4	-0.67	14.56	-28.83	8.60	9.92	9.74

Table 2. Relative rotation angles.

Master Cam1	Rotation angles (°)			Std. Dev. (°)		
	ω	φ	κ	ω	φ	κ
Slave Cam 2	179.330	0.108	0.594	0.060	0.068	0.028
Slave Cam 3	89.553	0.157	-0.221	0.058	0.055	0.056
Slave Cam 4	-90.263	0.031	-0.333	0.061	0.057	0.057

3.2 3D reconstruction results

Pilot One has successfully generated ceiling, floor, and wall parts for the indoor corridor area, with the majority of them being homogeneous objects. In the case of stitched images, 315 images were totally successfully aligned using a spherical camera model. However, there is a bending issue or banana effect along the corridor area (Fig. 5). Several methods exist to reduce these effects, such as input x, y, and z coordinates from GCPs measurement and increasing the number of GCPs with a balanced distribution. (Andaru et al. 2022). Due to data collection efficiency and the research area's constrained indoor space, the GCPs measurement approach is not appropriate for this case study. Therefore, this geometrical distortion was solved by incorporating the pre-calibrated parameters within the original images (i.e., a total of 774 pairs and 3096 original images). After that, 3D generation was produced without any bending issues (as shown in Fig.6). Additionally, only one of three parts (391/938) of all the original images in the study area could be successfully aligned using the datasets acquired with Sony α7R2 caused by homogeneous objects in the study area (depicted in Fig.7a). To ensure the cause of the images is not totally aligned, 714/714 images taken with a Sony α7R2 were perfectly aligned in the corridor area with more features (depicted in Fig.7b). Therefore, according to this finding, the multi-camera's calibrated ROPs are very beneficial for the alignment process, particularly in the homogeneous objects, whereas in a single full-frame camera, there is an issue during alignment process.

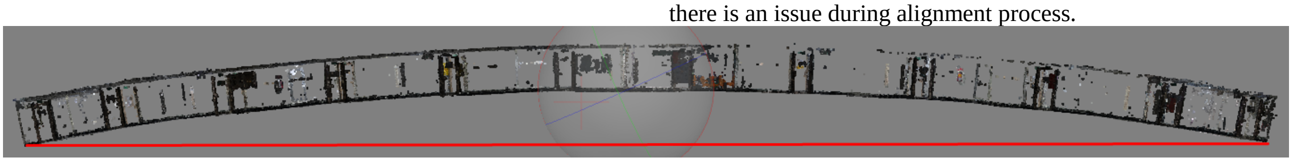

Figure 5. Sparse cloud from spherical images obtained banana effect, it caused by camera model and uncalibrated spherical images.

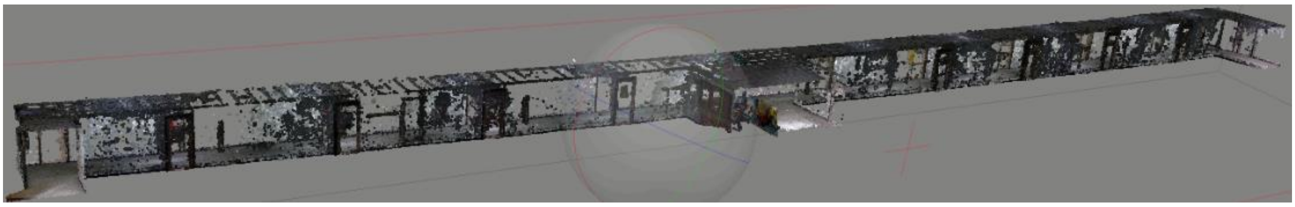

Figure 6. Dense cloud from unstitched and calibrated images with control scale bars to resolve the banana effect.

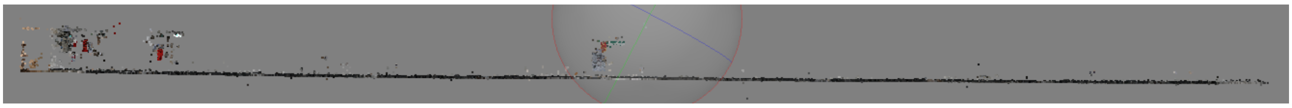

Figure 7. Sony α7R2 not perfectly aligned due to homogeneous object.

Figure 8. Sony α7R2 is applied to another corridor area with more features.

3.3 Accuracy assessment

The first step was to set up eight CSBs with four horizontal distributions, four vertical distributions, and 12 CkSBs to generate a 3D reconstruction. The length difference between the generated reconstruction and the reference data was obtained at 0.4 m (or 0.58% of 68.1 m), and the CkSBs error was 1.9 cm. The results were equally comparable when we changed the positions of eight CSBs. The length difference of the Pilot One camera result compared with TLS was 0.3 m (or 0.44% of 68.1 m) after we attempted to set up 10 CSBs with all horizontally and 10 CkSBs. The difference increases to 0.5 meters, or 0.73 of 68.1 meters, when we try to configure five CSBs with all in horizontal position.

Additionally, we try to use two CSBs in a variety of positions and orientations. First, in each of the four quarters of the study area, we set up two CSBs in a vertical orientation. We attempt to arrange two CSBs in a horizontal and vertical orientation. Similar to when we use eight CSBs, there is a length difference of 0.4 m (or 0.58% of 68.1 m). When we used 2 CSBs scenarios for this

study, we also obtained about 2 cm of CkSBs error. After that, we attempt two scale bars in horizontal orientation. This scenario yielded a 68.1 m length measurement which matches the TLS measurement. Fig.9 depicts the placement of two horizontal CSBs.
For comparison, we setup 20 CkSBs without any CSBs to simulate for future applications and yielded a 2.3 m (i.e., 3.37% of 68.1m) length estimation error, even though this trial only has 3.9 cm of CkSBs error (Fig. 10). The results demonstrate that even if the 3D dense point clouds do not exhibit the banana effects or bending issues, there is a difference if scale bars are not used due to rolling shutter effects of the proposed multi-camera rig system. However, because calibrated has been implemented in the multi-camera rig system, it is now only necessary to attempt for fewer CSBs (i.e., two) for future application where access may be limited. The CSBs amount, orientations, and length differences with ground truth for these various scalebar scenario configurations were described in (Table.3).

Figure 9. The most suitable scale bars placement in this experiment.

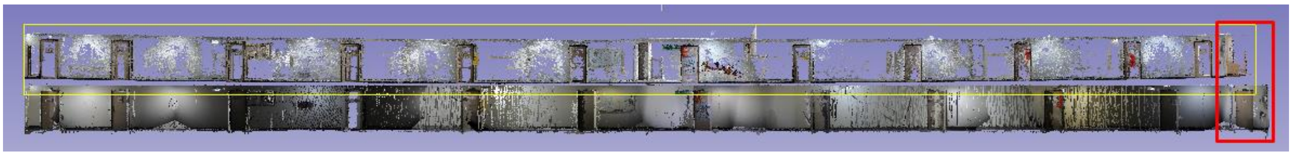
Figure 10. The difference between TLS and the calibrated unstitched images without control scale bars, it has obtained 3.38% of length error over a 68.1 m long corridor area.

Table 3. Control scale bars amount and orientations.

No	Control Scale Bars (CSBs)	Check Scale Bars (CkSBs)	Orientation of CSBs	CSBs error (cm)	CkSBs error (cm)	Length (m)	Length by TLS (m)	Difference (%)
1	0	20	-	-	3.99	65.8	68.1	3.377
2	2	18	1 hz & 1 ver	2.88	1.89	67.7	68.1	0.587
3	2	18	2 ver	1.68	1.94	67.7	68.1	0.587
4	8	12	4 hz & 4 ver	1.82	1.9	67.7	68.1	0.587
5	8	12	4 hz & 4 ver	1.86	1.94	67.7	68.1	0.587
6	5	15	5 hz	1.95	2.01	67.6	68.1	0.734
7	10	10	10 hz	1.89	1.83	67.8	68.1	0.441
8	2	18	2 hz	2.14	2.03	68.1	68.1	0.000

4. CONCULSIONS

This experiment simulates a proposed method of 3D reconstruction in an indoor long corridor by utilizing consumer-grade and portable instruments. By utilizing 360-degree coverage from four fisheye lenses equipped in a multi-camera rig system, it was possible to cover the entire corridor area with only a straight-line data acquisition as an efficient solution. Pre-calibration of IOPs and ROPs is useful to cope with weak and instable geometrical networks because these parameters are crucial to apply for future applications, especially in a long corridor area to produce reliable 3D reconstruction results.
Experimental results show that the suggested multi-fisheye camera-rig is considered a fast and cost-effective indoor image acquisition tool. The ROPs of a multi-fisheye camera-rig are critical not only for image alignment but also for 3D modelling without controls. In the experiment, the 3D model generated from stitched uncalibrated images has a geometrical issue by producing a banana effect. While the calibrated IOPs and ROPs from unstitched images are able to resolve the banana effect from spherical images in a long corridor area. In addition, instead of producing higher resolution with a full frame camera sensor, the image results were not totally aligned due to the homogeneous object. In this case, we can conclude that the increasing chance of alignment is another advantage for calibrated ROPs from multi-camera rig systems. Furthermore, the calibrated unstitched original images show that there is no significant length difference if we utilize eight CSBs or two CSBs. Therefore, producing calibrated ROPs camera calibration could also reduce the number of CSBs, which is beneficial for a long corridor area that is difficult to access. However, due to the rolling shutter effect, this experiment yielded 2.3 m (i.e., 3.37% of 68.1m) length estimation error if we configure without any control scale bars and utilize 20 CkSBs, even though this trial only has 3.9 cm CkSBs of Root Mean Square (RMS) error between 3D reconstruction measurement generated by Pilot One and scale bars length measured by tape measurement.

5. REFERENCES

Abate, D., I.Toschi, C.Sturdy-Colls, andF.Remondino. 2017. "A Low-Cost Panoramic Camera for the 3d Documentation of Contaminated Crime Scenes." *International Archives of the Photogrammetry, Remote Sensing and Spatial Information Sciences - ISPRS Archives* 42(2W8): 1–8.

AlKhalil, O. 2020. "Structure from Motion (SfM) Photogrammetry as Alternative to Laser Scanning for 3D Modelling of Historical Monuments." *Open Science Journal* 5(2).

Andaru, R., Rau, J.Y., Chuang, H., 2022. "Multitemporal UAV Photogrammetry For Sandbank Morphological Change Analysis: Evaluations of Camera Calibration Methods, Co-Registration Strategies, and the Reconstructed DSMs." *IEEE Journal of Selected Topics in Applied Earth Observations and Remote Sensing* 15: 5924–42.

Balletti, C., Guerra, F., Tsioukas, V., Vernier, P., 2014. “Calibration of Action Cameras for Photogrammetric Purposes.” *Sensors (Switzerland)* 14(9): 17471–90.

Barazzetti, L., Previtali, M., Roncoroni, F., 2017. “3D Modelling with the Samsung Gear 360.” *International Archives of the Photogrammetry, Remote Sensing and Spatial Information Sciences - ISPRS Archives* 42(2W3): 85–90.

Dawson, S, M., Hamish, B., Eva, L., Pascal, S. 2017. “Inexpensive Aerial Photogrammetry for Studies of Whales and Large Marine Animals.” *Frontiers in Marine Science* 4(NOV): 1–7.

Detchev, I., M.Mazaheri, S.Rondeel, and A.Habib. 2014. “Calibration of Multi-Camera Photogrammetric Systems.” *International Archives of the Photogrammetry, Remote Sensing and Spatial Information Sciences - ISPRS Archives* 40(1): 101–8.

Fausta, F., Limongiello,M., Palacios,B, J, F., 2016. “Testing GoPro for 3D Model Reconstruction in Narrow Spaces.” *Acta IMEKO* 5(2): 64–70.

Fraser, C. S., S.Al-Ajlounl. 2006. “Zoom-Dependent Camera Calibration in Digital Close-Range Photogrammetry.” *Photogrammetric Engineering and Remote Sensing* 72(9): 1017–26.

Fraser, Clive S. 1997. “Digital Camera Self-Calibration.” *ISPRS Journal of Photogrammetry and Remote Sensing* 52(4): 149–59.

Fraser, C. S. and Edmundson, K. L., 2000. "Design and implementation of a computational processing system for off-line digital close-range photogrammetry," *ISPRS Journal of Photogrammetry and Remote Sensing*, 55(2):94-104.

Habib, Ayman et al. 2006. “Stability Analysis of Low-Cost Digital Cameras for Aerial Mapping Using Different Georeferencing Techniques.” *Photogrammetric Record* 21(113): 29–43.

Hasler, O., B.Loesch, S.Blaser, S.Nebiker. 2019. “Configuration and Simulation Tool for 360-Degree Stereo Camera Rig.” *International Archives of the Photogrammetry, Remote Sensing and Spatial Information Sciences - ISPRS Archives* 42(2/W13): 793–98.

Jhan, J. P., Y. T.Li, and J. Y.Rau. 2015. “A Modified Projective Transformation Scheme for Mosaicking Multi-Camera Imaging System Equipped on a Large Payload Fixed-Wing UAS.” *International Archives of the Photogrammetry, Remote Sensing and Spatial Information Sciences - ISPRS Archives* 40(3W2): 87–93.

Jhan, J. P., J .Y. Rau, and C. M. Chou. 2020. “Underwater 3D Rigid Object Tracking and 6-DOF Estimation: A Case Study of Giant Steel Pipe Scale Model Underwater Installation.” *Remote Sensing* 12(16): 1–15.

Jiang, S., W. Jiang., Wei. Huang, and Liang.Yang. 2017. “UAV-Based Oblique Photogrammetry for Outdoor Data Acquisition and Offsite Visual Inspection of Transmission Line.” *Remote Sensing* 9(3).

Lari, Z., Ayman, H., Mehdi, M., Kalee,l, A., 2014. “Multi-Camera System Calibration with Built-in Relative Orientation Constraints (Part 2) Automation, Implementation, and Experimental Results.” *Journal of the Korean Society of Surveying Geodesy Photogrammetry and Cartography* 32(3): 205–16.

Perez, Alberto J., JavierPerez-Soler, Juan CarlosPerez-Cortes, andJose LuisGuardiola. 2022. “Improving Multi-View Camera Calibration Using Precise Location of Sphere Center Projection.” *Computers* 11(6): 1–11.

Pérez, M., F.Agüera, andF.Carvajal. 2012. “Digital Camera Calibration Using Images Taken From an Unmanned Aerial Vehicle.” *The International Archives of the Photogrammetry, Remote Sensing and Spatial Information Sciences* XXXVIII-1/C22(September): 167–71.

Sandro, E ., Woelk, F., Koch, R., 2007. “Calibration of a Multi-Camera Rig from Non-Overlapping Views.” *Lecture Notes in Computer Science (including subseries Lecture Notes in Artificial Intelligence and Lecture Notes in Bioinformatics)* 4713 LNCS: 82–91.

Wierzbicki, Damian. 2018. “Multi-Camera Imaging System for UAV Photogrammetry.” *Sensors (Switzerland)* 18(8).

Yamafune, K. 2017. “A Methodology for Accurate and Quick Photogrammetric Recording of Underwater Cultural Heritage.” *Proceedings of the 3rd Asia-Pacific Regional Conference on Underwater Cultural Heritage* 1: 517–37.